Soft Matter

ROYAL SOCIETY
OF CHEMISTRY | Celebrating IYPT 2019

PAPER
XiaoLu Geng *et al.*
The influence of pH, protein concentration and calcium
ratio on the formation and structure of nanotubes from
partially hydrolyzed bovine α-lactalbumin

Check for updates

The influence of pH, protein concentration and calcium ratio on the formation and structure of nanotubes from partially hydrolyzed bovine α-lactalbumin†

XiaoLu Geng, [iD] *[a] Jacob Judas Kain Kirkensgaard, [iD] [a] Lise Arleth,[b] Jeanette Otte[a] and Richard Ipsen [iD] [a]

Formation of nanotubes from partially hydrolysed α-lactalbumin (α-La) was investigated at five pH values, two concentrations of α-La and two calcium levels. Nanotubes were formed under almost all combinations of the investigated factors, and for the first time the formation of nanotubes at low pH (4.0) and low protein concentration (10 g l^{-1}) was observed. Only one sample (10 g l^{-1}, calcium ratio 2.4, and pH 7.5) formed mainly fibrils instead of nanotubes. By altering the three investigated factors, fibrils and/or aggregates were sometimes formed together with nanotubes resulting in transparent, semi-transparent, or non-transparent gels, or sediments. However, structural modelling based on small-angle X-ray scattering data indicated that the formed nanotubes were only to a minor degree affected by the investigated factors. The majority of the nanotubes were found to have an outer diameter of around 19 nm, an inner diameter of 6.6 nm and a wall thickness of 6.0 nm, except for three samples at low α-La concentrations and high calcium levels which exhibited slightly smaller dimensions. These three factors affected the hydrolysis as well as the self-assembly rate, resulting in the observed differences. However, these factors did not influence the architecture of the self-assembled nanotubes, and the lateral spacing of the individual parallel β-sheet motifs was found to be 1.05 ± 0. 03 nm for all nanotubes. This study provides novel fundamental knowledge of the formation and structure of α-La nanotubes under different conditions, which will facilitate future application of these nanotubes in food and pharmaceutical areas.

1. Introduction

Recently, it has been shown that self-assembly of several food grade proteins or peptides into highly ordered architectures at the nanometer scale is feasible after chemical or physical treatments of the protein molecules. The most frequently reported nanostructure formed by food proteins is amyloid fibrils, which is summarized in a recent review by Raynes *et al.*[1] Food proteins include the whey protein β-lactoglobulin (β-Lg),[2,3] hen egg white lysozyme (HEWL),[4,5] and several plant proteins.[6,7] Spherical or non-spherical shaped nanoparticles have also been reported formed by bovine serum albumin,[8] lactoferrin,[9] and other proteins. Compared to the amyloid fibrils mentioned above, the formation of nanotubes has been much less frequently reported. Until now, only two food proteins have been observed to form nanotubes, and these are the whey protein α-lactalbumin (α-La)[10] and HEWL.[11] These two structurally related proteins are globular proteins in their native state. For HEWL, the self-assembly of the protein molecule was induced by treatment at pH 2.0 and 90 °C for 30 h. This led to the denaturation of the protein forming mainly a random secondary structure, which in turn self-assembled longitudinally into amyloid fibrils. These fibrils grow laterally over time to form twisted ribbons, helical ribbons and finally nanotubes. The nanotubes formed by partially hydrolyzed bovine α-La at lower temperature are quite different. To the author's knowledge, the partially hydrolyzed α-La is the only food grade protein that has been reported to self-assemble into nanotubes with more or less retained secondary structure.[12–14] This phenomenon is very rare. When looking outside the food sector, only a few proteins or peptides have been found to maintain their globular structure while self-assembling into nanotubes, *i.e.* tubulins forming microtubules.[15,16] This might provide an opportunity for loading the tubes with different types of

[a] *Section for Ingredients and Dairy Technology, Department of Food Science, University of Copenhagen, Rolighedsvej 30, DK-1958 Frederiksberg C, Denmark. E-mail: xig@food.ku.dk*

[b] *X-ray and Neutron Science, Niels Bohr Institute, University of Copenhagen, Universitetsparken 5, 2100 København Ø, Denmark*

† Electronic supplementary information (ESI) available. See DOI: 10.1039/c9sm00127a

bio-functional components leading to potential innovation possibilities in the food and pharmaceutical areas.[17,18]

As the second major whey protein in bovine milk, α-La is traditionally used as a food ingredient due to its valuable functionalities in terms of nutrition and food structure. The ability of α-La to self-assemble into nanotubes after partial hydrolysis by Glu- and Asp-specific proteases from *Bacillus licheniformis* (BLP) at pH 7.5 and in the presence of calcium was discovered by Ipsen *et al.*[10] The nanotubes formed under these conditions were reported to have an outer diameter of 20 nm and an inner diameter of 8.7 nm.[19] The length can reach several micrometers,[19] and they elongate and entangle over time (4–6 h), ultimately forming transparent gels with strengths between 0.03 and 58 kPa depending on the conditions.[10,12]

The building fragments have been identified. With 123 amino acid residues in a chain held together by four disulphide bonds, α-La is initially hydrolyzed to form favorable building blocks with molecular masses ranging from 10 to 14 kDa (intact α-La has a mass of 14.2 kDa). One of the fragments f11-112, with a mass of 11.6 kDa, is believed to be the main building block.[12,20,21] The remaining three disulphide bonds in the fragments keep the structure spherical, but with a reduced size ($\approx$ 3.5 nm in diameter) compared to the intact α-La ($\approx$ 3.8 nm in diameter).[19] During the self-assembly process, initially, dimers of these fragments are formed through anti-parallel β-sheet hydrogen bonding. The dimers then self-assemble following a nucleation growth mechanism, *via* β-sheet stacking, resulting in a 10 start, right handed helical nanotubular structure.[12,20]

Many factors can influence the formation of α-La nanotubes. However, only a few have been studied, *i.e.* (i) the influence of α-La concentration, between 1% and 10%;[10,22] (ii) the molar ratio of Ca^{2+} to α-La (*R*), between 0 and 17;[23] and (iii) the pH value, between 4.0 and 7.5.[12] However, all studies have only focused on the impact of one parameter at a time. Since these three factors influence the rate of hydrolysis and/or the rate of self-assembly, it would be interesting to study the effect of these factors, to explore the conditions for the formation of protease-induced α-La nanotubes. In addition, it is also notable that the nanotube structure characterization was only carried out at pH 7.5 in previous studies. No knowledge is currently available on the size of nanotubes formed at a lower pH, which might be different since the altered net charge will affect the forces responsible for driving or preventing the event of self-assembly as well as the binding in the final structures.[12]

The objective of the present study is to explore the conditions for the formation of α-La nanotubes and gels, at two concentrations of α-La and calcium, and at five different pH values. Moreover, the nature of the nanotubes formed under the varying conditions is characterized by transmission electron microscopy (TEM) and small angle X-ray scattering (SAXS), the two methods widely used in the nanostructure characterization. They complement one another, with TEM providing information on individual structures, in two dimensions, and SAXS providing the average structural arrangement of the investigated system in three dimensions.

2. Experimental

2.1 Materials

Bovine α-La was purchased from Sigma-Aldrich (type I, L5385). The protease from *Bacillus licheniformis* (BLP) with an activity of 0.3 AU g^{-1} was kindly provided by Novozymes A/S (Bagsværd, Denmark). All other chemicals used in this study were of analytical grade.

2.2 Nanotube and gel formation

Bovine α-La and $CaCl_2$ were dissolved in 1 ml 75 mM HCl–Tris buffer at desired concentrations and pH values. Then the protein solutions were kept at 4 °C overnight for complete hydration. A brief naming of the samples is "protein concentration_calcium ratio_pH", where the protein concentration is 30 or 10 g l^{-1}, the calcium ratio is 2.4 or 5.4, and the pH values are 7.5, 7.0, 6.5, 5.5 and 4.0.

Before each experiment, the BLP solution was made by dissolving 3.6 mg BLP powder in 20 μl MilliQ water and subsequently 10 μl of this solution was added to 1 ml α-La solution providing a final enzyme/substrate ratio of 6% (w/w). All samples were incubated at 50 °C in a water bath for 6 h and subsequently cooled at room temperature for 30 min. Whether a gel was formed or not was determined visually by turning the vial upside down.

2.3 Transmission electron microscopy (TEM)

After cooling, 500 μl of the sample was immediately fixed by mixing with 500 μl of 1.5% of glutaraldehyde in 0.1 M sodium cacodylate buffer at pH 7.0, and left at room temperature for 1 h. The fixed samples were then diluted with 0.1 M sodium phosphate buffer to 6 g l^{-1} (samples containing 30 g l^{-1} protein) or 4 g l^{-1} (samples contain 10 g l^{-1} protein). The pH of the Na-phosphate buffer was 7.2 for samples with pH from 7.5 to 6.5, and 5.5 for samples with pH of 5.5 and 4.0. One drop of the sample was placed on a Formvar/carbon film grid, treated and examined using a Philips CM-100 electron microscope as described by Geng *et al.*[12] The ImageJ software[24] was used for measuring the diameter of the observed structures, using a plug-in tool (Vessel_width) by the method described by Liuhanena *et al.*[25] More than 10 nanotubes in each sample were randomly selected and the diameter was measured at five different places on each nanotube.

2.4 Small and wide angle X-ray scattering (SAXS and WAXS)

After the formation of nanotubes, a portion of each sample was loaded carefully into a vacuum-tight sample holder and sealed between 5 and 7 μm thick mica windows obtaining a sample thickness of 1.5 mm. The samples were investigated at room temperature using a SAXSLab instrument (JJ-X-ray, Copenhagen, Denmark) equipped with a 100 XL+ microfocus sealed X-ray tube (Cu-K$_\alpha$ radiation, Rigaku, The Woodlands Texas, USA) and a 2D 300 K Pilatus detector (Dectris Ltd, Baden, Switzerland). All the samples were initially measured at configuration I (WAXS) with a *q*-range of 0.07–2.96 Å^{-1} and then at configuration II (SAXS) with a *q*-range of 0.01–0.93 Å^{-1}. The scattering vector *q* is defined by

$q = 4\pi/\lambda \sin\theta$, where $\lambda = 1.54$ Å is the wavelength of the incoming beam, and θ is half of the scattering angle. Each measurement was taken under vacuum with an acquisition time of 60 min. The scattering spectra were azimuthally averaged to yield the scattering intensity as a function of q and absolute intensity calibration in units of 1 cm^{-1} was performed using the SAXSLab's direct standardless calibration method. Finally, buffer background subtraction was applied to generate the final scattering intensity $I(q)$.

2.5 Modelling of small-angle X-ray scattering data

The SAXS data were fitted by equation modelling the nanotubes as monodisperse hollow cylinders and the remaining unassembled large fragments from α-La (occurring as monomers, dimers and higher order oligomers) as polydisperse spheres, as explained below.

We assume that there is no structure factor contribution since the α-La concentration was relatively low (3% and 1%). Therefore, only the form factor was taken into account in the modelling of the scattering data.

The starting point in our modelling was the general equation for the scattering intensity per unit volume of a system of particles in solution

$$I(q) = \Phi_P V_P \rho^2 P_P(q) \tag{1}$$

where $\Delta\rho$, Φ_P, V_P and $P_P(q)$ are the excess scattering length density, the volume fraction, the molecular volume and the scattering form factor of the particle in question, respectively. Two contributions were included to describe the formed particles, one from hollow cylinders, $P_{HC}(q)$, to describe the formed nanotubes and another from polydisperse spheres, $P_S(q)$, to describe the unfibrillated fractions of the samples. Hence, the total intensity becomes

$$I(q) = \Delta\rho^2 \left[\Phi_S \int P_s(q,R) D(R) V_S(R) \mathrm{d}R + \Phi_{HC} V_{HC} P_{HC}(q) \right] \tag{2}$$

where $\Phi_S(q)$ and $\Phi_{HC}(q)$ denote the volume fractions of the spheres and hollow cylinders, respectively. Note that since the two contributions, spheres and hollow cylinders, are made from the same protein, their excess scattering length density $\Delta\rho$ can be assumed to be the same.

In eqn (2) the contribution from the polydisperse spheres is calculated *via* integration of the form factor, $P_S(q,R)$, of a sphere of radius R, volume $V_S(R) = 4/3\pi R^3$ and over a size distribution, $D(R)$. $P_S(q,R)$ and $D(R)$ are given by eqn (3) and (4), respectively,

$$P_s(q,R) = \left[3\frac{\sin qR - qR\cos qR}{(qR)^3} \right]^2 \tag{3}$$

and

$$D(R) = \frac{1}{R\sigma\sqrt{2\pi}} \exp\left(\frac{-[\ln(R/R_0)]^2}{2\sigma^2} \right). \tag{4}$$

Here $D(R)$ is described in terms of the log-normal distribution where σ is the variance and R_0 is the geometric mean of the log-normal distribution.

To calculate $P_{HC}(q)$ we note that for cylinders with axis ratio values larger than ~ 10, the form factor can be approximated by

the product of the longitudinal contribution to the form factor $P_L(q)$ and the cross sectional contribution to the cylinder form factor $P_{CS}(q)$,[26] thus

$$P_{HC}(q) = P_L(q)P_{CS}(q). \tag{5}$$

The longitudinal contribution to the form factor is given by the expression for an infinitely thin rod of length L

$$P_L(q) = 2\frac{\mathrm{Si}(qL)}{qL} - 4\frac{\sin^2(qL/2)}{q^2 L^2} \tag{6}$$

where

$$\mathrm{Si}(x) = \int_0^x \frac{\sin(t)}{t} \mathrm{d}t \tag{7}$$

and the form factor for the cross sectional contribution of hollow cylinders is given by

$$P_{CS}(q) = \left[2\frac{J_1(qR_o)}{qR_o} - 2\frac{J_1(qR_i)}{qR_i} \right]^2 \tag{8}$$

where $J_1(x)$ is the first order Bessel function of the first kind and R_o and R_i are the outer and inner radii of the hollow cylinder, respectively.

In order to relate the volume fractions of the two constituents to the absolute scattering intensity we note that the total volume fraction of the protein can be written as $\Phi_S = \Phi_T + \Phi_{HC}$. By defining dimensionless volume fraction ratios $\alpha = \Phi_T/\Phi_S$ and $\beta = 1 - \alpha = \Phi_{HC}/\Phi_T$ and introducing an overall scaling constant c to account for small uncertainties in the absolute intensity calibration, sample thickness, protein concentration and contrast, our effective model expression becomes

$$I(q) = c\Delta\rho^2 \Phi_T[\alpha P_{PS}(q) + (1-\alpha)V_{HC}P_{HC}(q)]. \tag{9}$$

$\Delta\rho^2$ and Φ_T are calculated from known quantities and kept fixed in the fits, and the scaling factor c is required to be close to unity. Using the value 0.1 e Å^{-3} for the excess electron density of protein in water, and 2.82×10^{-5} Å e^{-1} for the Thomson scattering length of an electron, the contrast is $\Delta\rho^2 = 7.95 \times 10^{-12}$ (Å Å^{-3})^2. The protein volume fraction is calculated using a protein mass density $\rho_{protein}$ of 1.35 g cm^{-3} and the concentration C so that $\Phi_T = C/\rho_{protein}$.

Appropriate unit conversions were applied everywhere to ensure that the scattering intensity in terms of scattering cross-section per unit volume was obtained in a final unit of cm^{-1}. The fits were done using an in-house MATLAB code by least-square χ^2-minimisation to optimize agreement between the model and the data. Thus, the free parameters in the model are the radius and variance of the polydisperse size distribution, the relative contributions of spheres and cylinders quantified by α and the inner and outer radii and in principle the length of the hollow cylinders. However, the experimentally accessible q-range does not permit the calculation of the actual cylinder lengths directly from the scattering data and it is therefore not possible to directly determine the amount of protein forming tubes and fractions respectively. We can however still qualitatively use α to measure where in our phase space the most mass is converted to tubes, only not in absolute numbers. We can,

however, circumvent this by using a non-tube forming sample as an internal reference as described below in Section 3.3.

3. Results and discussion

3.1 Appearance and microstructure of gels and nanotubes

The macroscopic appearance of the samples formed after 6 h of reaction was as a transparent gel, a semi-transparent gel, a non-transparent gel, a sediment, a clear liquid, or a blurry liquid depending on the applied conditions. A complete overview of the physical appearance of the samples is provided in Table 1. It is interesting to note that at a higher α-La concentration, with a low calcium ratio, all samples formed a gel – though with a less clear appearance as the pH decreased from 7.5. This is in accordance with the results in our previous study[12] using α-La purified from commercial whey protein concentrate (WPC). Also at a lower α-La concentration (10 g l^{−1}) gels were formed at pH 7.0 and at pH 6.5 at low Ca ratio (R = 2.4). To our knowledge this is the first report on BLP-induced gel formation from α-La at 10 g l^{−1}.

The nanostructures formed under the various conditions were observed by TEM. A full presentation of the TEM images of 20 samples is shown in Fig. S1 (ESI†), while some selected images are shown in Fig. 1 and 2. Surprisingly, 19 out of the 20 samples were found to form nanotubes. The details of the formation of nanotubes from α-La and the forces involved have been discussed previously.[12,20,21] The reason that one type of self-assembly structure, the nanotubes, can give rise to various states (Table 1) is the influence of the applied conditions, *i.e.* pH, calcium levels and α-La concentration, resulting in different

Table 1 Summary of the appearance of 20 samples after 6 h reaction[a]

[α-La] (g l^{−1})	Ca^{2+} ratio	pH values				
		7.5	7.0	6.5	5.5	4.0
30	2.4	Tr	Semi-tr	Semi-tr	Non-tr	Non-tr
	5.4	Semi-tr	Non-tr	Sedi	Sedi	Sedi
10	2.4	CL	Tr	Non-tr	Sedi	Sedi
	5.4	BL	Non-tr	Sedi	Sedi	Sedi

[a] The abbreviations used in the table are Tr: transparent gel, semi-Tr: semi-transparent gel, non-Tr: non-transparent gel, sedi: sedimentation, CL: clear liquid, and BL: blurry liquid.
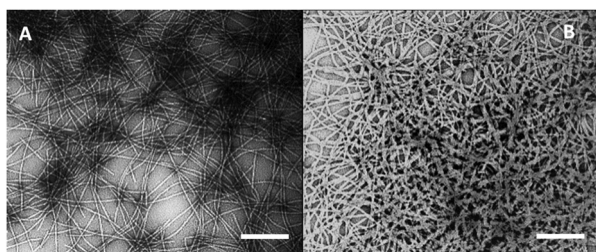

Fig. 1 TEM micrographs of transparent (A) and semitransparent (B) gel structures made from α-La nanotubes at an α-La concentration of 30 g l^{−1}, a calcium ratio of 2.4, and pH 7.5 (A) and pH 6.5 (B). The scale bar is 500 nm.
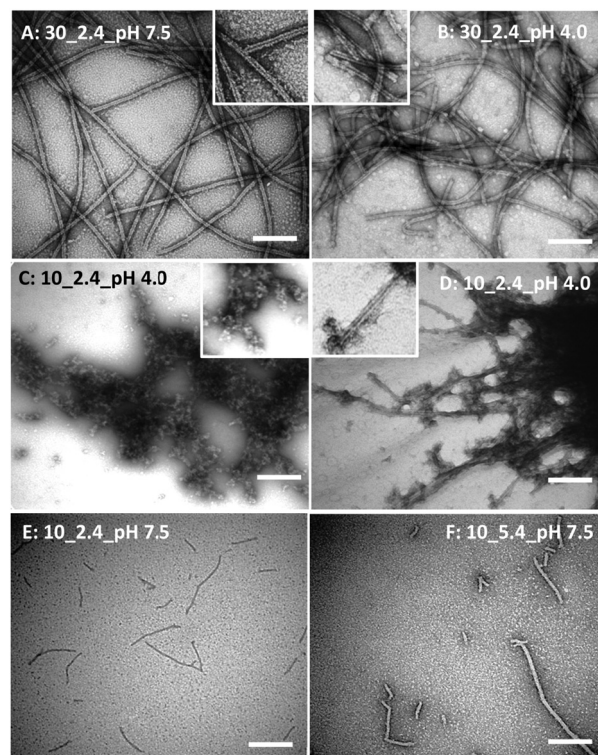

Fig. 2 Selected TEM micrographs showing nanotubular structures formed at different conditions with respect to α-La concentration (10 or 30 g l^{−1}), calcium ratio (2.4 or 5.4) and pH. The sample name is indicated after (A–F), the first number is the α-La concentration, the second number is the calcium ratio, and the third is the pH value. The insets in (A, B and D) show a dark line in the middle, indicating the hollow core of the nanotubes. Aggregates were also observed in some samples, one example is given in C. E shows the formation of fibrils and F shows the formation of very short nanotubes. Scale bar is 200 nm.

amounts and organizations of the nanotubes and other structures formed.

An example of the effect of pH on the organization of the nanotubes responsible for the transparent and semitransparent gels at high α-La and low calcium levels is shown in Fig. 1. At high pH, for example sample 30_2.4_pH 7.5 (Fig. 1A and 2A), long, straight, but also curved, tubes with a length of more than 1 μm were formed. The inset image in Fig. 2A shows a dark line in the middle of two lines, indicating the hollow core of the nanotube.[23] This is in good agreement with the results of the studies by Graveland-Bikker *et al.*,[14] and Ipsen *et al.*,[10] who used similar conditions. At pH 7.5, the increased rate of hydrolysis as compared to a lower pH[12] provides adequate building blocks, and a slower self-assembly[12,27,28] allowing the building blocks to sufficiently elongate into long nanotubes, hence a fine and more homogenous network is created (Fig. 1A). This allows light to pass through and therefore the gel appears transparent. Upon decreasing pH, the nanotubes became shorter and more curved (Fig. 2B). Similar nanotubes were observed at pH 4.0 with α-La being isolated from the WPC.[12] This might be due to the reduced electrostatic repulsion among the building blocks at a lower pH leading to an increased self-assembly rate[12] and

allowing a fast increase in the number of nanotubes. Hence, the growth of the nanotubes is interrupted by other nanotubes growing in other directions. Over time, the nanotubes overlapped and entangled forming a denser and more compact network which might be one of the reasons for the reduced gel transparency (Fig. 1B).

The level of free calcium also influenced the appearance of nanotubes and gels. Upon increasing the calcium ratio from 2.4 to 5.4, at all pH levels and at both α-La concentrations, the end products all changed to a more turbid appearance (Table 1). It is known that free calcium ions are essential for the formation of α-La nanotubes.[22] Calcium may act as a salt bridge connecting the carboxylate groups between different building fragments.[13,23] However, an excess amount of free calcium changes the spatial distribution of the strands to form amorphous structures and/or weak, turbid gels at pH 7.5.[10,23] In the current study, with the combination of a high level of calcium and low pH, most of the samples were found to exhibit phase separation. This is due to the accelerated self-assembly rate caused by both the high level of calcium[23] and the low pH values.[12] Thus, a large number of aggregates which are composed of very short and disorganized proto-fibrils (Fig. 2C) are formed and sediment together with α-La nanotubes (Fig. 2D).

In a system where the process of hydrolysis and self-assembly occur simultaneously, and when the concentration of the substrate is low enough, the hydrolysis rate will dominate hence limiting the self-assembling process.[29] This might be the case for sample 10_2.4_pH 7.5 in our study where the α-La concentration is only 10 g l^{-1}. No nanotubular structures were observed in the TEM images of this sample, instead, a small amount of short fibrils with a diameter of around 8 nm and a length of around 200 nm was observed (Fig. 2E). This is in line with the results reported by Otte et al.,[21] who showed Cryo-TEM images containing mainly fibrils from α-La under similar conditions. It is notable that, at this low α-La concentration, a small decrease in pH, from 7.5 to 7.0, led to the formation of many nanotubes and a fine-stranded, transparent gel (Table 1). Also, increasing the calcium ratio from 2.4 to 5.4 resulted in the formation of short (∼200 nm) nanotubes (Fig. 2F), however, no gel was formed (Table 1). This shows that small changes in the pH or the calcium level can tune the formation of nanotubes and gels from α-La at a concentration of 10 g l^{-1}. This might be useful from an economic point of view for further studies on their application.

3.2 Characterization of nanotubes by X-ray diffraction methods

3.2.1 SAXS data analysis.
In order to characterize the nanostructures in the formed samples after the hydrolysis and assembly reactions, we applied SAXS and interpreted the data using the mathematical model based on the existing knowledge of α-La nanotubes, as described in the Experimental section. The experimental scattering curves of the 20 samples are plotted in Fig. 3A. Eighteen of the 20 samples show a clear broad peak or oscillation around a q value of 0.043–0.046 Å^{-1}, followed by some smaller oscillations, showing the typical form factor of hollow cylinders with a structurally homogenous cross-section.
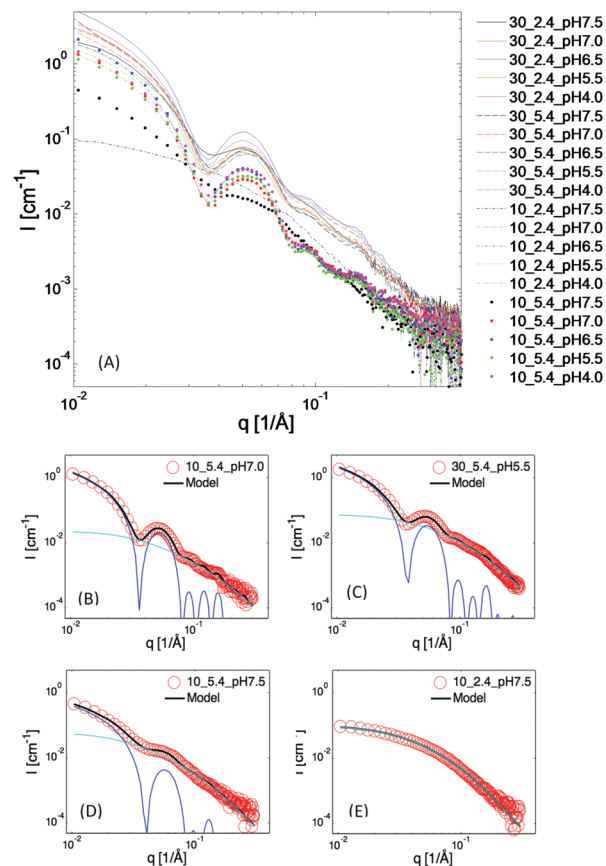

Fig. 3 (A) Normalized scattering curves of 20 samples after 6 hours of reaction at 50 °C with a protease from *Bacillus licheniformis*. (B–E) Examples after model fitting. The dark blue line represents the monodisperse hollow cylinder. The light blue line represents polydisperse spheres. The red circle indicates the data from experiments, and the black line is the data predicted from the model. The first number indicates the α-La concentration (30 or 10 g l^{-1}), and the second number indicates the calcium level, R = 2.4 or 5.4, followed by the pH value.

The peaks show only slight variations in the q position indicating that the diameters of the nanotubes varied very little. The SAXS data of all samples were fitted with the proposed model of monodisperse hollow cylinders with a remaining fraction of polydisperse spheres (eqn (2)). Examples of the obtained fits are shown in Fig. 3B–E. The model fitted the data from the samples with the form factor for hollow cylinders very well, based on the low χ^2 value (≤ 10) obtained for most samples. For example, for the sample 10_5.4_pH 7.0 shown in Fig. 3B, the model gave a quite high confidence ($\chi^2 = 2.5$) and the oscillations of the peaks were well captured. On the other hand, only four samples (30_5.4_pH 5.5, 30_5.4_pH 4.0, 10_2.4_pH 5.5, and 10_5.4_pH 4.0) gave χ^2 values ranging from 11 to 19. However, as shown in Fig. 2C, although the fitting has a confidence of $\chi^2 = 19.3$ for sample 30_5.4_pH 5.5, the fits appear to capture the features of the SAXS data well. This shows that the model can be used for characterizing the structure of the nanotubes.

The fits for the two samples that did not show the typical form factor for hollow cylinders are shown in Fig. 3D and E. Sample 10_5.4_pH 7.5 showed a less pronounced peak (Fig. 3A)

indicating less tube formation, which is in accordance with our TEM images shown in Fig. 2F. The fit in this case was also satisfactory as shown in Fig. 3D. Finally, judging from the shape of the scattering curve of sample 10_2.4_pH 7.5 (Fig. 3A), the structures in the solution should be spherical, with no nanotubes. This is confirmed by the model which fits very well with the polydisperse sphere model as seen in Fig. 3E. In this sample a small amount of short fibrils was also observed in the TEM images, but these are not reflected in the SAXS data. Modelling of the SAXS data of α-La nanotubes has been conducted previously by Graveland-Bikker et al.[19] for a sample that is very similar to sample 30_2.4_pH 7.5 in our study. The model was built based on polydispersed spheres and hollow cylinders with 10% polydispersity of the outer radius of the tubes, assuming a tube length of 1 μm. No signs of such polydispersity were observed in the present data, instead, as stated above, the series of higher order oscillations observed for several of the samples indicate that the hollow cylinders indeed have a very homogeneous cross-section. This observation is supported by the TEM images, which showed no large difference in the size of the nanotubes in each sample.

3.2.2 The dimensions of nanotubes. Initially, the outer diameters of the nanotubes were measured directly from TEM images, showing that the outer diameter of the nanotubes ranged from 20 to 37 nm (results not shown). During the sample preparation for TEM where the nanotubes were dried (vacuum), they may however have collapsed on the grid, which results in a maximum width of πr,[23,30,31] thus these numbers may not represent the actual nanotube diameter.

More precise measurements of the dimensions were, therefore, obtained from the SAXS measurements (as explained in Section 3.2.1), since the original nanostructures were kept in an aqueous environment. The fitting results of the dimensions of the nanotubes are shown in Fig. 4. In general, the nanotubes exhibited outer diameters of 17.8–19.4 nm, inner diameters of 5.1–7.4 nm, and deduced wall thicknesses of 5.1–6.6 nm. These dimensions are all in good agreement with the dimensions obtained previously[19] by modelling the SAXS data (outer diameter of 19.5–21 nm, inner diameter of about 6–10 nm, and wall thickness of 5.6 nm), of α-La nanotubes formed at 28 g l⁻¹, R = 3 and pH 7.5. It seems that in our study the dimensions of the nanotubes were more or less retained upon changing the pH, the α-La concentration and the calcium level, except for three samples, which were made at a low α-La concentration (10 g l⁻¹), a high calcium ratio (R = 5.4), and at pH 7.5, 5.5 and 4.0, respectively.

In order to elucidate the difference in the dimensions, the equation $R_1 \approx r_0(n/\pi - 1)$[32] was introduced, where R_1 is the inner radius of the nanotube, r_0 is the radius of the monomer (here we use the wall thickness divided by four), and n is the number of dimers in the transverse section. This resulted in three different nanotube configurations (Fig. 5). Fig. 5A shows the proposed transverse section of nanotubes, with packing of 10 dimers in a ring, obtained for the majority of the samples. This is in line with the α-La nanotube structure proposed by Graveland-Bikker et al.[20] It is interesting that these nanotubes all have similar dimensions: an outer diameter of around 19 nm,
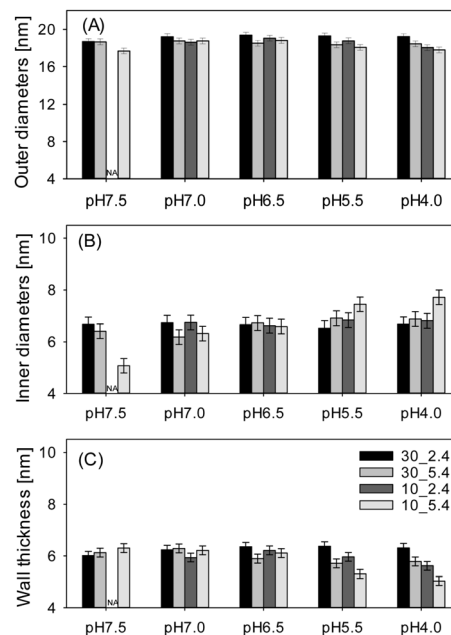
Fig. 4 The dimension of the nanotubes formed from α-La after 6 h of reaction at 50 °C with a protease from *Bacillus licheniformis*. The results are based on model fitting of the SAXS data; outer diameters (A), inner diameters (B) and wall thickness (C). Since only two independent measurements were performed for each sample during SAXS, the pooled standard deviations are shown as error bars. The legend is shown in C, the first number indicates the α-La concentration (30 or 10 g l⁻¹), and the second number indicates the calcium level, R = 2.4 or 5.4.

an inner diameter of around 6.6 nm, and a wall thickness of 6 nm, fitting well with the size of a dimer of hydrolyzed α-La. The reason may be that similar building fragments are formed under these conditions. Geng et al.[12] showed that the hydrolysis products formed at an α-La concentration of 30 g l⁻¹ and a calcium ratio of 2.4 were identical at varying pH values from 7.5 to 4.0. Since calcium has no influence on the hydrolysis process,[23] we assume that when increasing R to 5.4, the fragments would be the same as when R is 2.4. Nevertheless, at low α-La concentration, the influence of pH and calcium on the formation of building fragments is not known. One can speculate that, at an α-La concentration of 10 g l⁻¹ and R = 2.4, the nanotube building fragments should be well protected from further degradation due to the slow hydrolysis rate and the fast self-assembly rate prevailing at pH below 7.5, as shown previously for higher α-La concentrations.[12] Therefore, the nanotubes seem to be formed by similar fragments for all these conditions, hence a similar cylinder wall thickness.

The samples made at pH 7.5 with a low α-La concentration and a high R (10_5.4_pH 7.5) contained short nanotubes with significantly smaller dimensions (an outer diameter of 17.8 nm, a cavity of 5 nm and a wall thickness of around 6 nm). Since the wall thickness of the nanotubes in this sample is similar to that of the majority of the samples (Fig. 5A) we assume that they are formed from similar building fragments. Packing of the same dimer size as in most of the other nanotubes (Fig. 5A), around a small inner diameter, only allows 8 dimers in the transverse
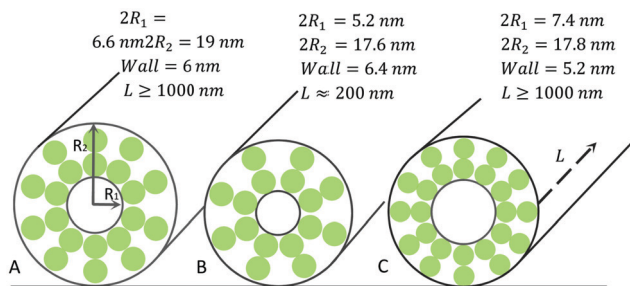
Fig. 5 A proposed schematic illustration shows the dimension and transverse structure of nanotubes. (A) Nanotubes with 10 dimers packed in a ring, representing 16 samples, which have similar dimensions. (B) Nanotubes with 8 dimers packed in a ring for samples with [α-La] = 10 g l⁻¹, calcium ratio R = 5.4 at pH 7.5. (C) Nanotubes with 12 dimers packed in a ring for samples with [α-La] = 10 g l⁻¹, calcium ratio R = 5.4 and at pH 5.5 and pH 4.0.

section nanotubes (Fig. 5B). The reason for the different architecture of packing is not clear, but it is obvious that the higher level of calcium plays an important role.[23] More work is needed to elucidate the reason.

The two samples made at a lower pH, but otherwise under the same conditions as the sample mentioned above (10_5.4_pH 5.5 and 10_5.4 pH 4.0) also had a smaller outer diameter but a larger inner cavity, and thus a thinner wall. This fits with packing of 12 smaller dimers around a cavity with a diameter of 7.4 nm (Fig. 5C). These nanotubes were formed under the most extreme conditions among the 20 samples, which could be the reason for the smaller fragments. At low α-La concentration and pH 5.5, the building fragments are less negatively charged. For example, at pH 7.5, the main building block (f12-113) has a charge of −7.5 and at pH 5.5 the charge is −4.3 (GPMAW 9.51; ©Lighthouse data 1992–2011, Odense, Denmark). The excessive Ca²⁺ may thus reduce the excess charge on the building fragments via counter-ion screening, which may lead to a more compact conformation of the building fragments.[33] Also the reduced electrostatic repulsion may increase the binding affinity between the building blocks which affects the underlying self-assembly mechanism.[34] At pH 4.0, where the protein is slightly positively charged, neutralization may be caused by the chloride ions by adding CaCl₂, which may also lead to a more compact conformation of the building blocks.

The difference in the number of dimers in the cross-section of the nanotubes may result in a different periodic pitch of the nanotubes, and hence the different architecture. In the case of β-Lg fibrils, the architecture of the nanofibrils can be tuned by altering the fine balance between electrostatic interactions and the elastic energy penalty associated with fibril twists.[35] Since the β-Lg fibrils were formed around pH 2.0, the electrostatic interactions were regulated by changing the ionic strength. In our study, the ionic strength was changed by adding surplus CaCl₂, and in addition, the charge was changed by altering the pH. These two factors together led to the difference in the size of the building fragments and the architecture of the nano-tubes. In addition, it is known[21] that one of the hydrophobic cores of α-La (the residues Phe31, His32, Gln117 and Trp118) is

exposed during the release of the terminal peptides, including residues Gln117 and Trp118, with the residues Phe31 and His32 remaining. This hydrophobic site is responsible for the formation of the dimeric building blocks. Such hydrophobic interactions are not expected to be influenced by the pH, the calcium level and the concentration of α-La. However, we cannot overrule that the hydrophobic interactions between the building blocks will influence the nanotubular architecture.

3.2.3 The *d*-spacing of nanotubes. Wide angle X-ray scattering (WAXS) was also applied to all 20 samples to investigate the nanotube structure at a more detailed level. Fig. 6 shows the scattering curves of WAXS measurements. It is interesting that 18 samples showed a small peak (Bragg peak) at the same q-value, around 0.596 Å⁻¹. Only the sample that did not form nanotubes (10_2.4_pH 7.5) and the sample that formed very short nanotubes (10_5.4_pH 7.5) did not show a detectable Bragg peak in WAXS. In order to reveal the details, the WAXS data around this peak (q ranges from 0.5 to 0.7 Å⁻¹) were normalized, as shown in the inset in Fig. 6. According to the equation for a Bragg peak ($d = 2\pi/q$), d was calculated to be 1.05 ± 0.03 nm for all 18 samples. Since the Bragg peak is used to describe the repeated space of the investigated structure, we assume that 1.05 nm is due to the β-sheet stacking of the building blocks in the nanotubes as previously described by Graveland-Bikker et al.[20] In their study, the d-spacing was obtained by Fourier transformation and projection of the Cryo-EM images of the nanotubes, showing a repeated space with a distance of 1.1 nm. Our WAXS results thus confirmed this value. Moreover, our results showed that this repeated spacing was not influenced by changing pH, α-La, and calcium levels, showing that under all conditions the nanotubes are formed with the same architecture, arranging the building blocks through β-sheet stacking.

Previously, d-spacing between β-sheets has been used to characterize amyloid fibrils, e.g. formed by short peptides
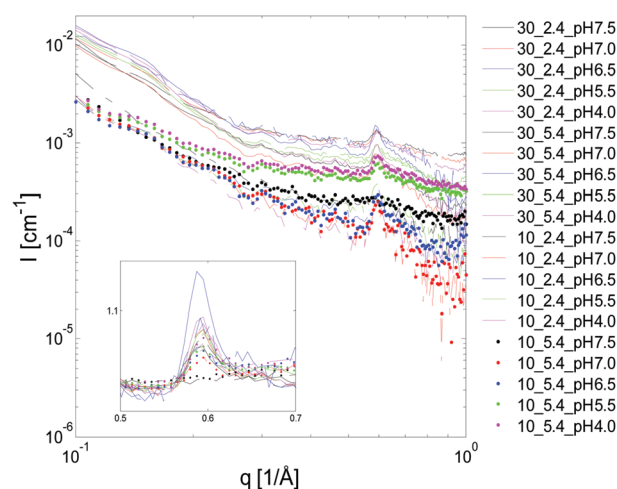

Fig. 6 The scattering intensity curve from the WAXS data. Inset: Showing the enlarged Bragg peak, and the data were normalized for this part of the data. The first number indicates the α-La concentration (30 or 10 g l⁻¹), and the second number indicates the calcium level, R = 2.4 or 5.4, followed by the pH value.

mainly containing β-sheets in their secondary structure.[36,37] These also gave a *d*-spacing of *ca.* 1 nm. Typically there is another repeated spacing of about 4.9 Å, which is the distance between the hydrogen bonds between each β-strand in the β-sheet. This is commonly known as the cross-β-sheet structure for the amyloid fibrils, due to the hydrogen bonded β-strands lying perpendicular to the fibril axis and forming the laminated β-sheets.[36] In our system, the 4.9 Å distance was not detected by the applied X-ray diffraction method, possibly due to the globular structure of the building blocks (containing other secondary structures besides β-sheets). It is surprising that a globular protein after hydrolysis to a suitable size of the fragment can also self-assemble into a similar amyloid structure.

3.3 Characterization of the remaining particles by SAXS

Besides the nanotubes, the hydrolysed α-La samples contained building fragments and other nanostructures, *e.g.* monomers, dimers, and very short fibrils or aggregates of hydrolysed α-La fragments. In the SAXS model (Section 3.2.1), we have considered these as polydisperse spheres to describe their mass and size.

Based on the SAXS analysis, it was possible to quantify the protein mass that goes into nanotubes and the protein remaining as spheres, respectively, assuming that all mass in the samples is in the form of tubes and fragments (even though there are also small amounts of fibrils present in some samples) and that the low *q* intensity level of the sphere contribution is less well defined than the much more intense tube signal. Since the sample 10_2.4_pH 7.5 shows no tubule formation, we can use this as a reference for 100% protein remaining in solution.

The relative mass of protein present as fragments (spheres) is found by calculating the quantity $M_{rel} = \alpha \times V_s$ for each sample, where V_s is the integrated volume from the sphere size distribution. All numbers are then normalized to the value from the non-tube forming the reference sample. The results are shown in Fig. 7A, plotted as a function of pH. Despite the assumptions made, we obtained reasonable results. The remaining protein mass for our sample 30_2.4_pH 7.5 was 42%, which compares well with the results obtained by Graveland-Bikker *et al.*,[19] for an analogous sample ($\approx$ 40% left in the solution). It is also notable that the samples with a low protein concentration, a high calcium ratio, and low pH values (10_5.4_pH 6.5, 10_5.4 pH 5.5 and 10_5.4 pH 4.0) had lower remaining protein masses, which is due to the fast self-assembly process under these conditions, causing nanotubes and other fragments to co-precipitate, thus leaving less remaining material in the supernatant.

The SAXS analysis also provides information on the size distribution of the remaining nanostructures in the samples. The diameters at the maximum probability of each sample are plotted in Fig. 7B. The sample made at high pH and low protein and calcium concentrations (sample 10_2.4_pH 7.5), which did not form any nanotubes, exhibited the largest spheres with a hydrodynamic diameter of around 3.4 nm. This is in good agreement with the expected size of the main building fragment with a mass of 11.6 kDa, since the intact α-La has a hydrodynamic diameter about 3.9 nm[38] and would be slightly reduced upon cleavage of the outer peptides. However, the size distribution of
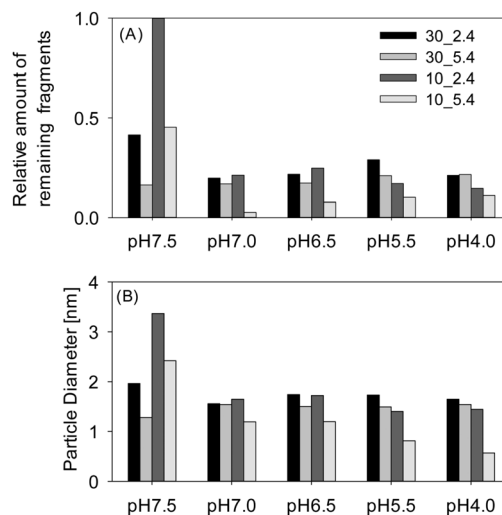

Fig. 7 Summary of the remaining particles in the solution. (A) Percentage of the remaining protein mass in the system, showing the amount of fragments which did not self-assemble into nanotubes. Sample 10_2.4_pH 7.5 did not form nanotubes, and hence it was used as a reference assuming that they contain 100% spheres. (B) The particle diameter at the maximum probability based on the log-normal size distribution of the spheres of all 20 samples. In the legend, the first number indicates the α-La concentration (30 or 10 g l⁻¹), and the second number indicates the calcium level, *R* = 2.4 or 5.4.

the spheres in this sample indicated a higher diversity of the hydrolysis products. This suggests that further degradation of the 11.6 kDa fragment might have reduced the concentration of this fragment below the threshold for nanotube formation. The diameters (at maximum probability) of the remaining spheres in the other 19 samples, which all formed nanotubes, ranged from 0.5 to 2.5 nm. These spheres probably result from further degradation of the main building fragment (11.6 kDa), and are too small to be integrated into nanotubes. The smallest diameters (less than 1 nm) for the remaining spheres were found in the two samples under extreme conditions (sample 10_5.4_pH 5.5 and 10_5.4 pH 4.0). Under these conditions, the very fast aggregation leads to sedimentation of larger fragments, leaving only very small particles in the solution.

Thus, the calcium and pH levels in the environment regulate the hydrolysis and the self-assembly rate, and hence which fragments can be integrated into nanotubes, and which cannot.

4. Conclusions

The conditions for formation of nanotubes from the partially hydrolyzed food grade protein, α-La, were explored in this study. We show the formation of nanotubes in a wide range of conditions including low concentration of α-La and low pH, something which has not been previously reported. By tuning the three important factors, pH, α-La and calcium concentration, the properties of the resulting hydrolysates can be controlled to form transparent, semi-transparent or non-transparent gels, as well as sediments due to the formation of not only nanotubes, but also other nanostructures including fibrils and random aggregates,
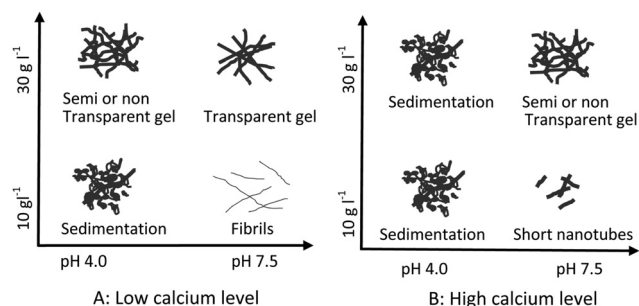
Fig. 8 Schematic summary of the formation of dominating nanostructure as influenced by pH, α-La and calcium concentrations. The unassembled protein fragments from α-La are also present under all conditions as polydisperse spheres, which are not illustrated in this figure. (A) Low calcium level R = 2.4 (R is the molar ratio between calcium and α-La). (B) High calcium level R = 5.4. The transparent gels are composed mainly of long, more than 1 μm, and slightly curved nanotubes, while the semi- and non-transparent gels are mainly composed of curved, overlapped and entangled nanotubes. Sedimentation occurs at high calcium levels and low pH due to the formation of fibrils and random aggregates, which associate with nanotubes. Under one condition (pH 7.5, 10 g l^{-1} α-La, R = 2.4) there is no nanotube formation, but fibrils. Under this condition, when the calcium level is increased (to R = 5.4), short nanotubes are formed.

as shown in Fig. 8. pH is a major regulator of the speed of the self-assembly, owing to its effect on the electrostatic interaction between the building fragments. It is also one of the key factors affecting the enzymatic hydrolysis, *i.e.* at low pH the hydrolysis is inhibited due to reduced enzyme activity.[12] The concentration of α-La determines the amount of nanotube building material. At low concentration, the hydrolysis rate dominates, thus less nanotube building blocks are available due to further degradation of the building blocks. Hence it limits the self-assembly process. Thus, a combination of the two factors, the pH and α-La concentration, regulates the species of fragments available for building of both nanotubes and fibrils. Surplus calcium may act to screen net charges resulting in a more compact conformation of the building fragments, and thus, influence the packing pattern of the nanotubes.

The developed model for SAXS data fitting was demonstrated to be useful to characterize the structure of α-La nanotubes in an accurate and efficient way. The dimensions of the majority of the nanotubes are not significantly influenced by altering the three parameters investigated in the study. Most nanotubes had an outer diameter of around 19 nm, an inner diameter of 6.6 nm, and a wall thickness of 6.0 nm, consistent with 10 dimers packed in the cross section of the nanotubes. Only in three samples, all at low α-La concentration and high calcium levels, were the dimensions affected.

It is also indicated that all nanotubes formed in this study assembled *via* the β-sheet lamination along the nanotube axis, irrespective of the pH, and α-La and calcium levels. The current study has broadened the conditions for α-La nanotube formation and characterized the structure of the resulting nanotubes. This may provide more opportunities for future applications as a thickening or gelling agent in food systems, as well as in non-food areas such as encapsulation, drug delivery, scaffolds for

tissue engineering, or as a template for nano-wires, and thus provides a base for further application of these food grade nanotubes in the food, pharmaceutical, materials science, and nanotechnology areas.

Conflicts of interest

There are no conflicts to declare.

Acknowledgements

Notes and references

1 J. K. Raynes, J. A. Carver, S. L. Gras and J. A. Gerrard, *Trends Food Sci. Technol.*, 2014, **37**, 42–50.
2 S. G. Bolder, H. Hendrickx, L. M. C. Sagis and E. van der Linden, *J. Agric. Food Chem.*, 2006, **54**, 4229–4254.
3 W. S. Gosal, A. H. Clark, P. D. A. Pudney and S. B. Ross-Murphy, *Langmuir*, 2002, **18**, 7174–7181.
4 S. Goda, K. Takano, K. Yutani, Y. Yamagata, R. Nagata and H. Akutsu, *et al.*, *Protein Sci.*, 2000, **9**, 369–375.
5 A. Cao, D. Hu and L. Lai, *Protein Sci.*, 2004, **13**, 319–324.
6 C. D. Munialo, A. H. Martin, E. van der Linde and H. H. J. de Jongh, *J. Agric. Food Chem.*, 2014, **62**, 2418–2427.
7 C. H. Tang and C. S. Wang, *J. Agric. Food Chem.*, 2010, **58**, 11058–11066.
8 M. M. A. Rodrigues, A. R. Simioni, F. L. Primo, M. P. Siqueira-Moura, P. C. Morais and A. C. Tedesco, *J. Magn. Magn. Mater.*, 2009, **321**, 1600–1603.
9 Z. H. Zhang, X. P. Wang, W. Y. Ayman, W. L. L. Munyendo, H. X. Lv and J. P. Zhou, *Drug Delivery*, 2013, **20**, 86–93.
10 R. Ipsen, J. Otte and K. B. Qvist, *J. Dairy Res.*, 2001, **68**, 277–286.
11 C. Lara, S. Handschin and R. Mezzenga, *Nanoscale*, 2013, **5**, 7197–7201.
12 X. L. Geng, M. J. Bjerrum, L. Arleth, J. Otte and R. Ipsen, *Int. Dairy J.*, 2016, **52**, 72–81.
13 Ö. Tarhan, E. Tarhan and S. Harsa, *J. Dairy Res.*, 2014, **81**, 98–106.
14 J. F. Graveland-Bikker and C. G. de Kruif, *Trends Food Sci. Technol.*, 2006, **17**, 196–203.
15 E. Nogales, S. G. Wolf and K. H. Downing, *Nature*, 1998, **391**, 199–202.
16 M. K. Gardner, B. D. Charlebois, I. M. Jánosi, J. Howard, A. J. Hunt and D. J. Odde, *Cell*, 2011, **146**, 582–592.

17 S. M. Lystvet, S. Volden, G. Singh, I. M. Rundgren, H. Wen, Ø. Halskau and W. R. Glomm, *J. Phys. Chem. C*, 2013, **117**, 2230–2238.

18 J. Xie, Y. Cao, M. Xia, X. Gao, M. Qin, J. Wei and W. Wang, *Adv. Healthcare Mater.*, 2013, **2**, 795–799.

19 J. F. Graveland-Bikker, G. Fritz, O. Glatter and C. G. de Kruif, *J. Appl. Crystallogr.*, 2006, **39**, 180–184.

20 J. F. Graveland-Bikker, R. I. Koning, H. K. Koerten, R. B. Geels, R. M. Heeren and C. G. de Kruif, *Soft Matter*, 2009, **5**, 2020–2026.

21 J. Otte, R. Ipsen, R. Bauer, J. M. Bjerrum and R. Waninge, *Int. Dairy J.*, 2005, **15**, 219–229.

22 R. Ipsen and J. Otte, *Biotechnol. Adv.*, 2007, **25**, 602–605.

23 J. F. Graveland-Bikker, R. Ipsen, J. Otte and C. G. de Kruif, *Langmuir*, 2004, **20**, 6841–6846.

24 C. T. Rueden, J. Schindelin and M. C. Hiner, *et al.*, *BMC Bioinf.*, 2017, 18–529.

25 S. Liuhanena, M. Sallisalmi, V. Pettilä, N. Oksala and J. Tenhunen, *Comput. Meth. Programs Biomed.*, 2013, **110**, 38–47.

26 J. S. Pedersen, *Modelling of small-angle scattering data from colloids and polymer systems*, Elsevier Science B. V., Amsterdam, 2002.

27 A. Ghosh, E. T. Dobson, C. J. Buettner, M. J. Nicholl and J. E. Goldberger, *Langmuir*, 2014, **30**, 15383–15387.

28 H. Zhang, Y. Liu, C. L. Wang, M. J. Li and B. Yang, *J. Phys. Chem. C*, 2008, **112**, 1885–1889.

29 A. Kroes-Nijboer, H. Sawalha, P. Venema, A. Bot, E. Flöter, R. den Adel, W. G. Bouwman and E. van der Linden, *Faraday Discuss.*, 2012, **158**, 125–138.

30 C. Lara, S. Handschin and R. Mezzenga, *Nanoscale*, 2013, **5**, 7197–7201.

31 K. Lu, J. Jaby, T. Pappannan, V. P. Conticello and D. G. Lynn, *J. Am. Chem. Soc.*, 2003, **125**, 6391–6393.

32 J. Adamcik and R. Mezzenga, *Marcromolecules*, 2011, **45**, 1137–1150.

33 M. Cornec, D. A. Kim and K. G. Narsimhan, *Food Hydrocolloids*, 2001, **15**, 303–313.

34 G. Lee, W. Lee, H. Lee, S. W. Lee, D. S. Yoon, K. Eom and T. Kwon, *Appl. Phys. Lett.*, 2012, **101**, 043703.

35 J. Adamcik and R. Mezzenga, *Soft Matter*, 2011, **7**, 5437–5443.

36 T. R. Jahn, O. S. Makin, K. L. Morris, K. E. Marshall, P. Tian, P. Sikorski and L. C. Serpell, *J. Mol. Biol.*, 2010, **395**, 717–727.

37 R. Nelson and D. Eisenberg, *Adv. Protein Chem.*, 2006, **73**, 235–282.

38 C. Redfield, B. A. Schulman, M. A. Milhollen, P. S. Kim and C. M. Dobson, *Nat. Struct. Biol.*, 1999, **6**, 948–952.